MISS CELIA M RODRIGUEZ-DOMINGUEZ (Orcid ID : 0000-0003-2352-0829)

Article type : MS - Regular Manuscript

Mapping xylem failure in disparate organs of whole plants reveals extreme resistance in olive roots

Celia M. Rodriguez-Dominguez, Madeline R. Carins Murphy, Christopher Lucani and Timothy J. Brodribb

School of Biological Sciences, University of Tasmania, Private Bag 55, Hobart, Tas. 7001, Australia

Author for correspondence:
Timothy J. Brodribb
Tel: +61 3 6226 1707
Email: timothyb@utas.edu.au

Received: *20 November 2017*
Accepted: *4 February 2018*

Summary

- The capacity of plant species to resist xylem cavitation is an important determinant of resistance to drought, mortality thresholds, geographic distribution and productivity. Unravelling the role of xylem cavitation vulnerability in plant evolution

and adaptation requires a clear understanding of how this key trait varies between the tissues of individuals and between individuals of species.

- Here we examine questions of variation within individuals by measuring how cavitation moves between organs of individual plants. Using multiple cameras placed simultaneously on roots, stems and leaves we were able to record systemic xylem cavitation during drying of individual olive plants.
- Unlike previous studies, we found a consistent pattern of root > stem > leaf in terms of xylem resistance to cavitation. The substantial variation in vulnerability to cavitation, evident among individuals, within individuals and within tissues of olive seedlings, was coordinated such that plants with more resistant roots also had more resistant leaves.
- Preservation of root integrity means that roots can continue to supply water for regeneration of drought-damaged aerial tissues after post-drought rain. Furthermore, coordinated variation in vulnerability between leaf, stem and root vulnerability in olive plants suggests a strong selective pressure to maintain a fixed order of cavitation during drought.

Key words: cavitation, leaf, olive, optical vulnerability method, root, stem, water stress, xylem.

Introduction

The accelerating rate of forest mortality worldwide in association with climate change weather events has injected new urgency into the challenge of understanding the cause of tree death during water stress. Large steps have been made recently towards this goal, with the identification of cavitation in the water transporting xylem tissue as a primary cause of plant mortality during drought (Bréda *et al.*, 2006; Brodribb & Cochard, 2009; Barigah *et al.*, 2013; Anderegg *et al.*, 2016; Adams *et al.*, 2017). New techniques that visualize the process of cavitation (the spread and formation of air embolisms in the continuous water column within the xylem that connects leaves with water in the soil) provide unequivocal evidence of the catastrophic nature of xylem failure during acute water stress (Brodersen *et al.*, 2013; Delzon & Cochard, 2014; Choat *et al.*, 2016; Brodribb *et al.*, 2016a,c; Ryu *et al.*, 2016; Torres-Ruiz *et al.*, 2016; Skelton *et al.*, 2017a). Xylem cavitation is not only linked to plant mortality,

but also to slow recovery after drought in forest trees (Brodribb *et al.*, 2010; Anderegg *et al.*, 2015b; Skelton *et al.*, 2017b), indicating the generality of this process in limiting plant growth, productivity and survival.

Species' ability to resist xylem cavitation appears to be adaptive, with strong correlations between xylem vulnerability and species rainfall niche indicating the central importance of this trait in species selection and community sorting (Blackman *et al.*, 2010; Jordan *et al.*, 2013; Brodribb *et al.*, 2014; Larter *et al.*, 2017). Growing recognition of xylem vulnerability as a core component in plant ecology has led to new hydraulic models being used to predict plant water use, mortality, productivity and plant competition (Diaz-Espejo *et al.*, 2012; McDowell *et al.*, 2013; Sperry & Love, 2015; Sperry *et al.*, 2016; Wolf *et al.*, 2016; Venturas *et al.*, 2017). However, a lack of information about variation in vulnerability within species and within individuals, largely due to hydraulic methodological limitations, remains a significant barrier to progress. The most well studied cases of variation in vulnerability within species come from work examining differences between root, stem and leaf tissues. Seminal work proposed the existence of hydraulic 'segmentation' within the tissues of plants (Zimmermann, 1978), such that peripheral tissues were hypothesised to be the first to become cavitated during drought, thereby protecting more costly tissues such as stems (Zimmermann, 1983; Tyree & Ewers, 1991). Recent work suggests that the magnitude of segmentation in conifers (Bouche *et al.*, 2016a) and herbaceous angiosperms (Skelton *et al.*, 2017a) is very small (Bouche *et al.*, 2016b), while there is some evidence that leaves (Charrier *et al.*, 2016) and flowers (Zhang & Brodribb, 2017) of woody angiosperms are more vulnerable to cavitation than stems.

Quantifying the magnitude of variation in xylem vulnerability within species and within individuals is fundamental for understanding whether species are likely to suffer localized cavitation leading to tissue death (such as leaf shedding) and reduced productivity, or if xylem cavitation is systemic, leading to catastrophic and lethal failure of the water transport system. However, major technical limitations have, until recently, prevented detailed exploration of this crucial question (Cochard *et al.*, 2013; Torres-Ruiz *et al.*, 2014; Brodribb, 2017). Root vulnerability to cavitation in particular has been significantly difficult to measure by traditional hydraulic methods due to the small size and fragility of the bulk of the root network, leading to conflicting results (Froux *et al.*, 2005; Hukin *et al.*, 2005; Johnson *et al.*, 2016). A recent shift towards visual methods in plant hydraulics, however, is

providing exciting new insights into the processes of cavitation and tissue deformation in roots (Cuneo *et al.*, 2016), stems (Choat *et al.*, 2016), leaves (Brodribb *et al.*, 2016a,b; Scoffoni *et al.*, 2016) and even flowers (Zhang & Brodribb, 2017). X-ray computed tomography (CT), cryo-SEM and optical light methods allow the xylem to be viewed in its natural state and under high water tension, thus preserving air bubbles and cell deformations that affect the flow of water during water stress.

Here we examine variation in xylem vulnerability within and among individual plants of a drought-resistant species, *Olea europaea*. An important aim was to measure xylem cavitation simultaneously at multiple points in individual plants (leaf, stem and root) to determine if large cavitation events occurred simultaneously (spread of cavitation) in major tissues of a droughted plant, or whether different organs had distinctive vulnerability characteristics. In addition, we compared the variation in vulnerability among individuals to determine if all tissues in more resistant individuals were coordinated to maintain a conserved order of cavitation within the plant. We chose olive as a test species because it represents the opposite end of the plant functional spectrum to the recently studied tomato, where all tissues were found to be similarly vulnerable to cavitation (Skelton *et al.*, 2017a). Olive is recognized as a 'model' hardy sclerophyll (Connor, 2005; Carr, 2013; Fernández, 2014), and thus our data for this species provides a comparison for the unexpected lack of segmentation found in a herbaceous annual (Skelton *et al.*, 2017a).

We hypothesized that core plant tissues (stems and coarse roots) should be the most important organs to preserve during drought, and should thus be the most resistant to cavitation. We also expected that any variation in vulnerability between individuals should be coordinated between tissues, for example, individuals with more resistant stem xylem should also exhibit more resilient leaf and root xylem to preserve a degree of segmentation in the plant body.

Materials and Methods

Plant material and growing conditions

Two-year-old olive seedlings (*Olea europaea* L. var. Kalamata, varietal clones propagated from stem cuttings) were grown in glasshouse facilities at the University of Tasmania from February to June in 2017. Following acquisition from a local nursery and 1 month before starting the experiment, all seedlings were replanted to 2-l pots using a 3 : 1 mixture of

coarse river sand and potting mix. Special care was taken during this procedure to avoid damaging the roots. Seedlings were then housed in a glasshouse where day : night temperatures were 23°C : 15°C, photoperiod was 16-h (supplemented and extended in the morning and evening by sodium vapour lamps, ensuring a minimum 200 µmol m^{-2} s^{-1} at the pot surface during the day period) and relative humidity was *c*. 40%. Pots were irrigated daily to fully supply their water requirements and to avoid any water stress that could cause xylem cavitation and result in the appearance of embolisms. Seedlings ranged from 70 to 120 cm in height.

Sample preparation

The day before xylem monitoring began, each seedling was moved to the laboratory and abundantly watered. Before commencing image capture, seedlings were removed from pots and their roots gently washed to remove most of the soil and accelerate desiccation during the measurements. Plants, with their roots under water, were covered with moist plastic bags and kept in the dark for *c*. 1 h to ensure stomatal closure and allow water potential equilibration. During sample preparation, all roots were submerged under water in a deep container and covered with wet paper towel to prevent any desiccation while the other plant organs were prepared to be monitored (in the case of visualizing cavitation events with the optical method) or measured (by following water status with a stem psychrometer). Entire seedlings were always used to monitor cumulative xylem embolisms. The monitoring process was performed in dark conditions and only the plant organs from which images were captured were illuminated. A total of nine plants were used to visually quantify root, stem and leaf midrib vulnerability to cavitation. For three plants, all three organs were simultaneously monitored (Fig. 1). The following section explains the preparation of an olive seedling in which the three organs were monitored. Additionally, a tenth plant, identically prepared, was used to concomitantly monitor six leaves from three different branches.

Optical vulnerability curves

Plant water potential A stem psychrometer (PSY1, ICT International, Armidale, NSW, Australia) was first installed on a central region of the main stem of the seedling within an internode of at least 3.5 cm in length. In the flattest part of that segment, a square of bark, sufficient for fitting the psychrometer, was carefully removed under a dissecting microscope

using a rigid razor blade to avoid any damage to the xylem. The psychrometer was then clamped to the stem and sealed air-tight with parafilm. The Peltier cooling time was adjusted from 5 s (when the plant was well hydrated) to a maximum of 30 s (as plant dehydrated) to ensure a sufficient volume of water was condensed onto the thermocouple and then evaporated to produce a stable reading of the wet-bulb depression temperature. Stem water potential (Ψ_{tem}) was recorded every 20 min and leaf water potential was periodically measured using a Scholander-type pressure chamber (PMS Instrument Company, Albany, OR, USA) to validate plant water status. We found a good agreement between both measurements (Supporting Information Fig. S1) and used the continuous measurements from the psychrometers to generate the optical vulnerability curves. Under the experimental conditions presented here, plants were not connected to soil and stomata were closed during the drying process, so there was no reason to expect hydraulic disequilibrium between tissues, until massive cavitation allowed tissues to become compartmentalized. Due to the large overlap in cavitation profiles between organs, we are confident that this scenario did not evolve in olive. Furthermore, the validation of stem psychrometer values with leaf water potential measured with the Scholander chamber, provided strong support that organs were well equilibrated during drying. A technical limitation of these stem psychrometers was that the lowest measurable water potential was -10 MPa. However, at those levels of water stress, turgor pressure was totally lost and most of the plants and organs had already passed their P_{50}, so it is unlikely that the rate of decreasing water potentials would change after this point. Therefore, linear regressions were fitted to the psychrometer data *vs* time (see the Image capture and analysis subsection) to extrapolate the water potential data beyond -10 MPa. Multiple linear regressions were used as required if the rate of decrease in water potential varied over time. A change in rate usually occurred before reaching -5 MPa.

Stem preparation Current-year shoots, avoiding those with active growth, and thus, living xylem, were selected to monitor cavitation events at stem level. A stem segment (internode) *c*. 1.5–2.0 cm in length was prepared by carefully removing the bark to expose undamaged xylem. Xylem depth was ascertained beforehand by sectioning and examining stem cross-sections to determine the optimal amount of bark to remove. Although not tested in the present work, recent studies have shown that stem girdling did not affect the xylem

integrity (Van de Wal *et al.*, 2017). In that case, the authors tested heat girdling in an herbaceous species (tomato), while in our study we did not heat the un-barked stems and we measured a woody plant, so stem xylem should not be affected by the bark removal. The diameter of stem xylem monitored was *c*. 1.5–3.0 mm. Immediately after positioning the seedling on the laboratory bench with its root and leaf midrib arranged for image capture (explained below), a custom built OpenSourceOV (OSOV; http://www.opensourceov.org) clamp was installed and firmly attached to the stem to minimize sample movement during the monitoring process. Materials and suppliers, instructions, image capturing and post image processing using OSOV devices, as well as an overview of the optical method, is explained in detail at http://www.opensourceov.org. Briefly, the sample is securely clamped in a 3D-printed enclosure and images are captured over time through a ×20 hand lens magnifier using a small 8 megapixel Raspberry Pi camera illuminated using six bright LEDs. The capture sequence is orchestrated using a Python script (Python Software Foundation. Python Language Reference, version 2.7) running on a connected Raspberry Pi microcomputer (Raspberry Pi Foundation, http://www.raspberrypi.org).

Leaf preparation Leaves from current-year shoots were used to visualize cavitation events in the leaf midrib (main vein of the olive leaf vasculature). Trichomes were removed from the abaxial surface using clear tape. A thin layer of the epidermal tissue surrounding the leaf midrib was cut longitudinally and removed under a dissecting microscope using a flexible razor blade to allow an unobstructed view of the xylem. Several tests were performed beforehand on leaf cross-sections to ascertain the optimal amount of tissue to remove to expose the xylem without inducing any damage (any damage to the xylem was immediately visible upon cutting). The diameter of leaf midrib xylem monitored ranged from 380 to 800 µm, and *c*. 1.5 mm in length. Before positioning the sample under the microscope, the leaf was sat on top of a rectangular piece of glass, fixed in place with tape, and the midrib covered with hydrogel (Tensive Gel, Parker USA). A cover glass was then placed over the hydrogel, and gentle force applied to dispel any bubbles in the gel, and adhere it to the glass. Images were collected with a Zeiss AxioCam HRc camera (Carl Zeiss, Gottingen, Germany) connected to a light microscope (Axioskop 2 plus, Carl Zeiss) at ×5 magnification. Midribs were illuminated with a custom-built 3D-printed LED mount with six bright LEDs attached to the objective lens (PAR at the surface of the leaf *c*. 400 µmol m^{-2} s^{-1}).

Root preparation After removing the wet paper towel from the root organ, a portion was submerged under water in a petri dish and a suberized root *c*. 1 mm in diameter was selected and a section of bark was carefully removed under a dissecting microscope using a syringe needle to expose the xylem. As with the other organs, tests were performed beforehand to identify the optimal amount of bark to remove to visualize the root xylem. The diameter of the root xylem monitored ranged from 460 to 700 µm, and from 1 to 2 mm in length. The root was prepared in a similar way to the leaf, that is, the root was fixed on top of a piece of glass, covered with hydrogel and topped with a coverslip. Images were collected with a Nikon DS-L1 digital camera connected to a microscope (Axiolab, Carl Zeiss) at ×4 magnification. The root was illuminated using a second 3D-printed LED mount attached to the objective lens (PAR at the surface of the sample *c*. 400 µmol m^{-2} s^{-1}).

Image capture and analysis Images from the three organs were collected using reflected light every 5 min during the drying process until no cavitation events were observed for at least 12 h and a maximum of 4 d (eight out of 10 individuals were allowed to further dehydrate for >1 d after the last cavitation event was observed). Recent studies (Skelton *et al.*, 2017a; Hochberg *et al.*, 2017) have reported the appearance of cavitation events long after stomatal closure. In the case of olive species, stomata appear to close at leaf water potential *c.* -1.50 to -2.00 MPa (Torres-Ruiz *et al.*, 2015; Hernandez-Santana *et al.*, 2016). Considering the long dehydration time allowed for each individual and the measured water potentials, we can be confident that the stomata were closed early during dehydration. Image sequences were then analysed according to Brodribb *et al.* (2016b, 2017). Briefly, total embolism was quantified by first determining pixel differences between images using ImageJ (Schindelin *et al.*, 2012) by subtracting the pixel values of each image from the next i.e. pixel values that do not change result in a value of zero. Noise was removed using the ImageJ outlier removal and pixel thresholding was used to extract embolism from any background noise remaining. Embolism area per image was calculated as the sum of non-zero pixels and expressed as cumulative embolisms, a percentage of total embolism area in the sequence. Cavitation spread or propagation can be observed directly. Linear regressions were fitted to the psychrometer data (stem water potential *vs* time) to derive stem water potential Ψ_{stem} (MPa) at the time of image capture. Ψ_{stem} (MPa) was plotted against

cumulative embolisms (% of total) and P_{50} (the Ψ_{stem} at which 50% of the xylem cavitation events have been observed) determined by fitting a sigmoid using the equation (Pammenter & Vander Willigen, 1998):

$$\text{Cumulative embolisms} = 100 / (1 + \exp(a\,(\Psi_{stem} - P_{50}))) \quad \text{Eqn 1}$$

P_{50} was derived for each sample. A total of six roots, seven stems and six leaf midribs were measured. Spatiotemporal colour maps of cavitation formation were created for some of the samples by colouring the embolism area in each sequence using a colour scale of Ψ_{stem} over time (Fig. S2).

Within individual variation in leaf vulnerability To further understand the variability of leaf vulnerability to cavitation, six leaves from three different branches from an entire individual olive seedling, prepared identically to the other seedlings, were concurrently monitored using a flatbed scanner (Perfection 800, Epson). In this case, leaves remained intact and only trichomes were removed from the abaxial leaf surfaces. Images were collected using transmitted light every 9 min (the minimum time required to scan all leaves once in sequence). Changes in light refraction due to cavitation events were recorded by monitoring the midrib at the adaxial surface. The procedure described above was used to build optical vulnerability curves. In addition, the distance of each leaf to the root was measured.

Xylem anatomy

Cross sections of the same root, stem and leaf midrib tissues monitored for cumulative embolisms were examined to explore the relationship between xylem anatomical dimensions and vulnerability to cavitation. Samples from each plant organ was stored at -20°C once monitoring had finished. Thin sections through the xylem were made using a freeze microtome. Sections were stained with 5% toluidine blue, and mounted on glass microscope slides in phenol glycerine jelly. Xylem dimensions of the three plant organs were measured using a Zeiss AxioCam HRc camera connected to a light microscope (Axioskop 2 plus, Carl Zeiss) at ×40 magnification for stems and ×100 magnification for roots and leaf midribs. Only vessels with lumen breadths > 9 µm were measured as smaller vessel were unlikely to be observed through the optical devices. None of the cross sections of the

monitored plant tissues presented any xylem damage. Lumen breadth (*b*) and wall thickness (*t*) were measured in 23–118 conduits per root sample, 85–139 conduits per stem sample, and 97–150 conduits per midrib sample. For each vessel, two measurements (maximum and minimum) were taken and averaged for *b* and *t* values. If vessel geometry approximates a cylindrical tube, $(t/b)^3$ is a measure of the cell vulnerability to collapse (Brodribb & Holbrook, 2005).

Statistics

One-way analysis of variance (ANOVA) was used to determine the statistical significance of organ type mean P_{50} ± SE estimated by fitting the Pammenter equation to the optical vulnerability curves obtained from roots (*n* = 6), stems (*n* = 7) and leaf midribs (*n* = 6) of nine olive seedlings. Mean comparisons were performed by post-hoc Tukey's test ($P < 0.05$).

Results

Cavitation events in roots, stems and leaf midribs were easily visualized using the optical method. The use of multiple cameras and microscopes to simultaneously record xylem cavitation across the plant body, from leaves to roots of olive seedlings (Fig. 1) provided the first view of how xylem cavitation spreads within plants. In all tissues, the larger cavitation events were larger than the single largest vessels, indicating that discrete events propagate radially and axially in the xylem (Supporting Information Fig. S3). Plots of cumulative xylem embolisms vs stem water potential (Ψ_{stem}) (Fig. 2) indicated considerable variation in the water potential at which 50% of cavitation events were visualized (P_{50}), both between and within plants. Estimates of P_{50} for roots ranged from -5.38 to -8.98 MPa (*n* = 6), from -4.15 to -8.99 for stems (*n* = 7), and from -3.13 to -7.04 MPa for leaf midribs (*n* = 6). After pooling vulnerability data for each organ across individuals, the roots were identified as the most resistant organ to cavitation (P_{50} = -7.10 ± 0.62 MPa), followed by stems (P_{50} = -5.67 ± 0.68 MPa), while the leaf midribs were significantly more vulnerable (P_{50} = -4.76 ± 0.67 MPa) (Fig. 3).

Comparing the vulnerability of each organ per individual among individuals, revealed coordination within individuals. Individuals with highly resistant stems also exhibited roots with the highest cavitation resistance and *vice versa* (Fig. 4). Leaf midribs followed the same trend, but high and uniformly distributed variation weakened relationships with the other

organs. More importantly, the order of cavitation between plant organs when the three organs were simultaneously monitored was always, from least to most resistant: leaf midribs > stems > roots (upper panels of Fig. 4). The strongest correlation between the P_{50} of measured organs was found between roots and stems (Fig. 5), indicating a greater and more conserved link between these two organs rather than leaves. No examples of major cavitation events propagating instantaneously between organs were observed in the cumulative embolism plots (Fig. 4). However, there were some examples of smaller overlapping events in the embolism plots, particularly at the commencement of cavitation, where three out of seven specimens exhibited a synchronous first recorded cavitation (arrows in Fig. 4) **[Author, please confirm amended text 'three out of seven' is correct]**.

Of all measured organs, the leaf P_{50} was most variable between individuals. So to test the degree of within-individual variability in leaf P_{50}, we monitored six leaves distributed in three different branches from a single entire seedling (Fig. 6). P_{50} among leaves ranged substantially, from -5.82 to -6.96 MPa and was within the same range measured in leaf midribs from other seedlings (inset Figure in Fig. 6). Within the crown of the individual, more vulnerable leaves were found to occur further from the roots. Distance from the roots in this young plant was presumed to be an inverse proxy for leaf age (Supporting Information Fig. S4).

Across all tissues none of the measured xylem anatomical measurements were found to be correlated with P_{50} (Fig. 7). However, trends in xylem wall thickness, and $(t/b)^3$, in leaf midribs followed the expected pattern, with more resistant P_{50} weakly associated with thicker xylem cell walls.

Discussion

Plant distribution and mortality after extreme climatic events can be predicted based on species vulnerability to cavitation (Brodribb *et al.*, 2014; Anderegg *et al.*, 2015a; Skelton *et al.*, 2015; Adams *et al.*, 2017), yet uncertainty in the magnitude of variation in vulnerability within and between individuals of a species limits the confidence with which mortality thresholds can be defined. By using new camera technology to capture cavitation *in situ*, we were able to make the first examination of cavitation as it moves between the organs of an individual plant. Attaching multiple miniature cameras to leaves, stems and roots of individual plants revealed the timing of cavitation spread between organs and the degree of

continuity between organs. Four key findings were identified: a consistent ranking of root > stem > leaf in terms of xylem resistance to cavitation; variation between individuals was coordinated, for example, resistant leaves were attached to resistant roots; cavitation events were largely contained within organs, with few examples of large events connecting between tissues; variation in vulnerability among leaves within a single crown was observed, but it was small compared to variation between leaves of different individuals.

The optical vulnerability (OV) method provided a clear picture of embolism accumulation in all major tissues of 2-yr-old olive seedlings by allowing us to simultaneously examine cavitation spread through adjacent leaf, stem and root tissue. Cross validation of this technique with hydraulic methods in stems (Brodribb *et al.*, 2017) and leaves (Brodribb *et al.*, 2016b) gives confidence that the proxy measurement of 'area cavitated' faithfully represents percentage loss of hydraulic conductance measured by flow methods. In particular, our average P_{50} for stems (-5.67 MPa) agrees with the average P_{50} obtained by hydraulic methods (benchtop dehydration method) and X-ray micro-CT in the olive species (-5.70 MPa) (Ennajeh *et al.*, 2008; Torres-Ruiz *et al.*, 2014, 2017), validating the optical vulnerability method, at least at stem level, in olive, a narrow, long-vesselled species. Optical P_{50} did not agree with the much higher vulnerability for olive stems produced by methods involving stem excision, supporting the probability of artefacts associated with these methods for measuring species with relatively long vessels such as olive (Torres-Ruiz *et al.*, 2014, 2017).

Cavitation events were clearly visible in all tissues including the course roots of olive plants, providing a clear indication that the xylem in coarse roots was the last tissue to cavitate in the plant (Fig. 3). This result stands in contrast to many early studies that have suggested roots were more vulnerable to cavitation in angiosperm and conifer species (Sperry & Saliendra, 1994; Sperry & Ikeda, 1997; Kavanagh *et al.*, 1999) than the downstream organs. Attempts to explain these counter-intuitive observations, in terms of hydraulic segmentation, have led to suggestions that root cavitation should decouple the plant from the desiccating effects of the drying soil during drought (Domec *et al.*, 2009). More recent work using *in situ* assessment of air embolism suggest only very small differences in vulnerability between organs in tomato (Skelton *et al.*, 2017a) or even the suggestion that roots (Cuneo *et al.*, 2016) may be more resistant to cavitation than stems (Choat *et al.*, 2010) in grape. This kind of gradient in resistance may be an adaptation to

maximise recovery potential after rewatering by preserving xylem integrity in the roots. Indeed, of the traits that were found to correlate with environmental water stress across species in a recent meta-analysis, root hydraulic traits were some of the most strongly correlated with drought (Bartlett *et al.*, 2016).

Unlike previous studies that reported contrasting results in olive species (roots and leaves more vulnerable to cavitation than stems; Torres-Ruiz *et al.*, 2015), here we measured root, stem and leaf tissue simultaneously on the same (single-stemmed), intact olive plants. The within-plant control enabled, by using multiple cameras on a single plant combined with the non-invasive nature of the OV method, the highest confidence in our data. The sequence of vulnerability was not related to xylem conduit dimensions (Fig. 7), and only the thickness of the leaf midrib xylem cell walls and the index that dictates cell vulnerability to collapse, $(t/b)^3$, appeared to weakly correlate with leaf P_{50}, similar to results in Blackman *et al.* (2010). In addition, the observed strong relationship between the xylem vulnerability to cavitation at root and stem levels (Fig. 5) suggests a conservative link between these tissues that makes sense in terms of preserving the capacity to recover growth from core tissues (coarse roots and stems) upward (Pratt *et al.*, 2010).

It is interesting to note that there were few instances of large cavitation events propagating between tissues, despite their close proximity (plants were *c*. 1 m from root to leaf), indicating a degree of segmentation between tissues did exist in these plants. Although maximum vessel length in olive has been reported to be > 0.8 m in stems (Torres-Ruiz *et al.*, 2014), only very few vessels are expected to be continuous between stems and either the midrib, or the small roots where observations were made. Assuming the general theory that larger vessels are more vulnerable to cavitation (Sperry *et al.*, 2007), these longer vessels may have constituted the few initial cavitation events in individuals that often occurred simultaneously in the different tissues. The fact that the majority of cavitations did not occur simultaneously among tissues indicates that bubbles did not move instantly between axially connected vessels, and that vessel endings provided a temporal barrier for bubble propagation (Sperry *et al.*, 2006). This discontinuity between vessels explains the ability for different tissues within an individual to exhibit different cavitation thresholds.

Despite a large range of vulnerability observed among the 10 individuals of olive measured here, a strict conservation of relative cavitation thresholds was observed among tissues. Even though the vulnerability of olive stems and roots were not significantly

different among individuals (Fig. 3), examination within individuals revealed a clear correlation between the vulnerability of these tissues compared by individual (Figs 4, 5). This apparent coordination of vulnerability between tissues suggests that the developmental changes likely to be responsible for modifying xylem vulnerability have a systemic effect across the plant. Such a result is perhaps not surprising considering that adaptation of the xylem to drier conditions, for example, would only be effective if all tissues changed vulnerability in unison.

The application of the OV method to examine the range of vulnerabilities expressed in a single plant reinforced the importance of variation within the olive species. A range of >1 MPa in P_{50} was measured among six leaves of an individual plant (Fig. 6). It is likely that leaf age may have played a part in the variation within the individual (Fig. S3), much in a similar way as variation in vulnerability has been noted between different ages of wood within a single stem (Melcher *et al.*, 2003; Rosner *et al.*, 2006). However, we did not find any relationship between plant age and mean P_{50} during the 5 months of data collection in olive, indicating a lack of any general age related trend in our plants (Fig. S5). Such variation within individuals is consistent with the concept of producing a staged loss of hydraulic function during the dehydration, which is presumably less catastrophic than the type of systemic embolism failure that would occur in an individual where all tissues shared a common cavitation threshold. Moreover, this behaviour might be an adaptive mechanism that allows olive to preserve core tissues (roots and stems) as long as possible to enable re-sprouting during more favourable conditions. The ability to produce new growth via dormant buds situated beneath the bark seems to be more frequent in woody plant species that grow in severe and frequently disturbed sites, like olive (Bellingham & Sparrow, 2000; Del Tredici, 2001). The OV method opens the possibility to further explore the generalization of this phenomenon beyond the olive species context and within a wider spectrum of plant functional groups.

The ability to describe propagation of cavitation within individual plants adds new physiological information to be incorporated in new model frameworks for drought-induced plant mortality (Martin-StPaul *et al.*, 2017). Considering the mean P_{50} for olive obtained in the present study (-6.18 MPa, average from all roots, stems and leaf midribs P_{50} measured) it is clear that this species falls among the most cavitation-resistant angiosperms that have been measured (Choat *et al.*, 2012), meaning that the species should survive extremely dry

conditions. However, given the degree of variation within and among individuals of a single olive variety, precise predictions about the timing of tissue damage and plant mortality during water stress of an individual plant require more specific information from the individual. This variation appears larger than the P_{50} reported previously using the widely accepted 'bench drying' method. However, the parallel variation reported here in root, stem and leaf midrib P_{50} in individuals and its coordination provide good verification that this variation in individuals of olive seedlings is not associated with artefact. Considering that the former method pools data from a large number of branches compared with the single branches used by the OV method, it is possible that intraspecific variation has been smoothed by previous methods. An interesting implication of the coordination in the high degree of variation noted here in P_{50} among individuals is that plasticity may play an important role in determining vulnerability and segmentation in olive plants. The optical method provides an excellent means by which this fascinating question might be addressed in the future.

Acknowledgements

This work was funded by the Australian Research Council, Discovery Projects, DP170100761. We thank Michelle Lang for glasshouse assistance and Luis Marrufo Perez for excellent design ideas.

Author contributions

T.J.B. and C.M.R-D. conceived the experiment. T.J.B., C.M.R-D. and M.R.C.M. designed the experiment. M.R.C.M. and C.L. contributed assisting with the optical vulnerability method. C.M.R-D. collected and analysed the data. T.J.B. and C.M.R-D. wrote the manuscript with revisions from M.R.C.M. and C.L.

References

Adams HD, Zeppel MJB, Anderegg WRL, Hartmann H, Landhäusser SM, Tissue DT, Huxman TE, Hudson PJ, Franz TE, Allen CD, *et al.* 2017. A multi-species synthesis of physiological mechanisms in drought-induced tree mortality. *Nature Ecology & Evolution* **1**: 1285–1291.

Anderegg WRL, Flint A, Huang C-Y, Flint L, Berry JA, Davis FW, Sperry JS, Field CB. **2015a**. Tree mortality predicted from drought-induced vascular damage. *Nature Geoscience* **8**: 367–

371.

Anderegg WRL, Klein T, Bartlett M, Sack L, Pellegrini AFA, Choat B, Jansen S. **2016**. Meta-analysis reveals that hydraulic traits explain cross-species patterns of drought-induced tree mortality across the globe. *Proceedings of the National Academy of Sciences, USA* **113**: 5024–5029.

Anderegg WRL, Schwalm C, Biondi F, Camarero JJ, Koch G, Litvak M, Ogle K, Shaw JD, Shevliakova E, Williams AP, *et al.* 2015b. Pervasive drought legacies in forest ecosystems and their implications for carbon cycle models. *Science* **349**: 528–532.

Barigah TS, Charrier O, Douris M, Bonhomme M, Herbette S, Améglio T, Fichot R, Brignolas F, Cochard H. **2013**. Water stress-induced xylem hydraulic failure is a causal factor of tree mortality in beech and poplar. *Annals of Botany* **112**: 1431–1437.

Bartlett MK, Klein T, Jansen S, Choat B, Sack L. **2016**. The correlations and sequence of plant stomatal, hydraulic, and wilting responses to drought. *Proceedings of the National Academy of Sciences, USA* **113**: 13098–13103.

Bellingham PJ, Sparrow AD. **2000**. Resprouting as a life history strategy in woody plant communities. *Oikos* **89**: 409–416.

Blackman CJ, Brodribb TJ, Jordan GJ. **2010**. Leaf hydraulic vulnerability is related to conduit dimensions and drought resistance across a diverse range of woody angiosperms. *New Phytologist* **188**: 1113–1123.

Bouche PS, Delzon S, Choat B, Badel E, Brodribb TJ, Burlett R, Cochard H, Charra-Vaskou K, Lavigne B, Li S, *et al.* 2016a. Are needles of Pinus pinaster more vulnerable to xylem embolism than branches? New insights from X-ray computed tomography. *Plant, Cell & Environment* **39**: 860–870.

Bouche PS, Jansen S, Sabalera JC, Cochard H, Burlett R, Delzon S. **2016b**. Low intra-tree variability in resistance to embolism in four Pinaceae species. *Annals of Forest Science* **73**: 681–689.

Bréda N, Huc R, Granier A, Dreyer E. **2006**. Temperate forest trees and stands under severe drought: a review of ecophysiological responses , adaptation processes and long-term consequences. *Annals of Forest Science* **63**: 625–644.

Brodersen CR, McElrone AJ, Choat B, Lee EF, Shackel KA, Matthews MA. **2013**. *In vivo* visualizations of drought-induced embolism spread in *Vitis vinifera*. *Plant Physiology* **161**: 1820–1829.

Brodribb TJ. **2017**. Progressing from 'functional' to mechanistic traits. *New Phytologist* **215**: 9–11.

Brodribb TJ, Bienaimé D, Marmottant P. **2016a**. Revealing catastrophic failure of leaf networks under stress. *Proceedings of the National Academy of Sciences, USA* **113**: 4865–4869.

Brodribb TJ, Bowman DJMS, Nichols S, Delzon S, Burlett R. **2010**. Xylem function and growth rate interact to determine recovery rates after exposure to extreme water deficit. *New Phytologist* **188**: 533–542.

Brodribb TJ, Carriqui M, Delzon S, Lucani C. **2017**. Optical measurement of stem xylem vulnerability. *Plant Physiology* **174**: 2054–2061.

Brodribb TJ, Cochard H. **2009**. Hydraulic failure defines the recovery and point of death in water-stressed conifers. *Plant Physiology* **149**: 575–584.

Brodribb TJ, Holbrook NM. **2005**. Water stress deforms tracheids peripheral to the leaf vein of a tropical conifer. *Plant Physiology* **137**: 1139–1146.

Brodribb TJ, McAdam SAM, Jordan GJ, Martins SCV. **2014**. Conifer species adapt to low-rainfall climates by following one of two divergent pathways. *Proceedings of the National Academy of Sciences, USA* **111**: 14489–14493.

Brodribb TJ, Skelton RP, Mcadam SAM, Bienaimé D, Lucani CJ, Marmottant P. **2016b**. Visual quantification of embolism reveals leaf vulnerability to hydraulic failure. *New Phytologist* **209**: 1403–1409.

Brodribb TJ, Skelton RP, McAdam SAM, Bienaimé D, Lucani CJ, Marmottant P. **2016c**. Visual quantification of embolism reveals leaf vulnerability to hydraulic failure. *New Phytologist* **209**: 1403–1409.

Carr MK V. 2013. The water relations and irrigation requirements of olive (*Olea europaea* L.): a review. *Experimental Agriculture* **49**: 597–639.

Charrier G, Torres-Ruiz JM, Badel E, Burlett R, Choat B, Cochard H, Delmas CEL, Domec J-C, Jansen S, King A, *et al.* 2016. Evidence for hydraulic vulnerability segmentation and lack of xylem refilling under tension. *Plant Physiology* **172**: 1657–1668.

Choat B, Badel E, Burlett R, Delzon S, Cochard H, Jansen S. **2016**. Noninvasive measurement of vulnerability to drought-induced embolism by X-ray microtomography. *Plant Physiology* **170**: 273–282.

Choat B, Drayton WM, Brodersen C, Matthews MA, Shackel KA, Wada H, McElrone AJ.

2010. Measurement of vulnerability to water stress-induced cavitation in grapevine: a comparison of four techniques applied to a long-vesseled species. *Plant, Cell & Environment* **33**: 1502–1512.

Choat B, Jansen S, Brodribb TJ, Cochard H, Delzon S, Bhaskar R, Bucci SJ, Feild TS, Gleason SM, Hacke UG, *et al.* 2012. Global convergence in the vulnerability of forests to drought. *Nature* **491**: 752–755.

Cochard H, Badel E, Herbette S, Delzon S, Choat B, Jansen S. **2013**. Methods for measuring plant vulnerability to cavitation: a critical review. *Journal of Experimental Botany* **64**: 4779–4791.

Connor DJ. **2005**. Adaptation of olive (*Olea europaea* L.) to water-limited environments. *Australian Journal of Agricultural Research* **56**: 1181–1189.

Cuneo IF, Knipfer T, Brodersen CR, McElrone AJ. **2016**. Mechanical failure of fine root cortical cells initiates plant hydraulic decline during drought. *Plant Physiology* **172**: 1669–1678.

Del Tredici P. **2001**. Sprouting in temperate trees: a morphological and ecological review. *Botanical Review* **67**: 121–140.

Delzon S, Cochard H. **2014**. Recent advances in tree hydraulics highlight the ecological significance of the hydraulic safety margin. *New Phytologist* **203**: 355–358.

Diaz-Espejo A, Buckley TN, Sperry JS, Cuevas MV, de Cires A, Elsayed-Farag S, Martin-Palomo MJ, Muriel JL, Perez-Martin A, Rodriguez-Dominguez CM, *et al.* 2012. Steps toward an improvement in process-based models of water use by fruit trees: a case study in olive. *Agricultural Water Management* **114**: 37–49.

Domec JC, Noormets A, King JS, Sun G, McNulty SG, Gavazzi MJ, Boggs JL, Treasure EA. **2009**. Decoupling the influence of leaf and root hydraulic conductances on stomatal conductance and its sensitivity to vapour pressure deficit as soil dries in a drained loblolly pine plantation. *Plant, Cell & Environment* **32**: 980–991.

Ennajeh M, Tounekti T, Vadel AM, Khemira H, Cochard H. **2008**. Water relations and drought-induced embolism in olive (*Olea europaea*) varieties 'Meski' and 'Chemlali' during severe drought. *Tree Physiology* **28**: 971–6.

Fernández JE. **2014**. Understanding olive adaptation to abiotic stresses as a tool to increase crop performance. *Environmental and Experimental Botany* **103**: 158–179.

Froux F, Ducrey M, Dreyer E, Huc R. **2005**. Vulnerability to embolism differs in roots and

shoots and among three Mediterranean conifers: consequences for stomatal regulation of water loss? *Trees – Structure and Function* **19**: 137–144.

Hernandez-Santana V, Rodriguez-Dominguez CM, Fernández JE, Diaz-Espejo A. **2016**. Role of leaf hydraulic conductance in the regulation of stomatal conductance in almond and olive in response to water stress. *Tree Physiology* **36**: 725–735.

Hochberg U, Windt CW, Ponomarenko A, Zhang Y-J, Gersony J, Rockwell FE, Holbrook NM. **2017**. Stomatal closure, basal leaf embolism, and shedding protect the hydraulic integrity of grape stems. *Plant Physiology* **174**: 764–775.

Hukin D, Cochard H, Dreyer E, Thiec D Le, Bogeat-Triboulot MB. **2005**. Cavitation vulnerability in roots and shoots: does *Populus euphratica* Oliv., a poplar from arid areas of Central Asia, differ from other poplar species? *Journal of Experimental Botany* **56**: 2003–2010.

Johnson DM, Wortemann R, McCulloh KA, Jordan-Meille L, Ward E, Warren JM, Palmroth S, Domec J. **2016**. A test of the hydraulic vulnerability segmentation hypothesis in angiosperm and conifer tree species. *Tree Physiology* **36**: 983–993.

Jordan GJ, Brodribb TJ, Blackman CJ, Weston PH. **2013**. Climate drives vein anatomy in Proteaceae. *American Journal of Botany* **100**: 1483–1493.

Kavanagh KL, Bond BJ, Aitken SN, Gartner BL, Knowe S. **1999**. Shoot and root vulnerability to xylem cavitation in four populations of Douglas-fir seedlings. *Tree Physiology* **19**: 31–37.

Larter M, Pfautsch S, Domec J-C, Trueba S, Nagalingum N, Delzon S. **2017**. Aridity drove the evolution of extreme embolism resistance and the radiation of conifer genus *Callitris*. *New Phytologist* **215**: 97–112.

Martin-StPaul N, Delzon S, Cochard H. **2017**. Plant resistance to drought depends on timely stomatal closure. *Ecology Letters* **116**: 519–532.

McDowell NG, Fisher RA, Xu C, Domec JC, Hölttä T, Mackay DS, Sperry JS, Boutz A, Dickman L, Gehres N, *et al.* 2013. Evaluating theories of drought-induced vegetation mortality using a multimodel-experiment framework. *New phytologist*: 304–321.

Melcher PJ, Zwieniecki MA, Holbrook NM. **2003**. Vulnerability of xylem vessels to cavitation in sugar maple. Scaling from individual vessels to whole branches. *Plant Physiology* **131**: 1775–1780.

Pammenter NW, Vander Willigen C. **1998**. A mathematical and statistical analysis of the curves illustrating vulnerability of xylem to cavitation. *Tree Physiology* **18**: 589–593.

Pratt RB, North GB, Jacobsen AL, Ewers FW, Davis SD. **2010**. Xylem root and shoot hydraulics is linked to life history type in chaparral seedlings. *Functional Ecology* **24**: 70–81.

Rosner S, Klein A, Wimmer R, Karlsson B. **2006**. Extraction of features from ultrasound acoustic emissions: a tool to assess the hydraulic vulnerability of Norway spruce trunkwood? *New Phytologist* **171**: 105–116.

Ryu J, Hwang BG, Kim YX, Lee SJ. **2016**. Direct observation of local xylem embolisms induced by soil drying in intact *Zea mays* leaves. *Journal of Experimental Botany* **67**: 2617–2626.

Schindelin J, Arganda-Carreras I, Frise E, Kaynig V, Longair M, Pietzsch T, Preibisch S, Rueden C, Saalfeld S, Schmid B, *et al.* 2012. Fiji: an open-source platform for biological-image analysis. *Nature Methods* **9**: 676–682.

Scoffoni C, Albuquerque C, Brodersen CR, Townes S V., John GP, Cochard H, Buckley TN, McElrone AJ, Sack L. **2016**. Leaf vein xylem conduit diameter influences susceptibility to embolism and hydraulic decline. *New Phytologist* **213**: 1076–1092.

Skelton RP, Brodribb TJ, Choat B. **2017a**. Casting light on xylem vulnerability in an herbaceous species reveals a lack of segmentation. *New Phytologist* **214**: 561–569.

Skelton RP, Brodribb TJ, McAdam SAM, Mitchell PJ. **2017b**. Gas exchange recovery following natural drought is rapid unless limited by loss of leaf hydraulic conductance: evidence from an evergreen woodland. *New Phytologist* **215**: 1399–1412.

Skelton RP, West AG, Dawson TE. **2015**. Predicting plant vulnerability to drought in biodiverse regions using functional traits. *Proceedings of the National Academy of Sciences, USA* **112**: 5744–5749.

Sperry JS, Hacke UG, Feild TS, Sano Y, Sikkema EH. **2007**. Hydraulic consequences of vessel evolution in angiosperms. *International Journal of Plant Sciences* **168**: 1127–1139.

Sperry JS, Hacke UG, Pittermann J. **2006**. Size and function in conifer tracheids and angiosperm vessels. *American Journal of Botany* **93**: 1490–1500.

Sperry JS, Ikeda T. **1997**. Xylem cavitation in roots and stems of Douglas-fir and white fir. *Tree Physiology* **17**: 275–280.

Sperry JS, Love DM. **2015**. What plant hydraulics can tell us about responses to climate-change droughts. *New Phytologist* **207**: 14–27.

Sperry JS, Saliendra NZ. **1994**. Intra- and inter-plant variation in xylem cavitation in *Betula occidentalis*. *Plant, Cell & Environment* **17**: 1233–1241.

Sperry JS, Wang Y, Wolfe BT, Mackay DS, Anderegg WRL, McDowell NG, Pockman WT. **2016**. Pragmatic hydraulic theory predicts stomatal responses to climatic water deficits. *New Phytologist* **212**: 577–589.

Torres-Ruiz JM, Cochard H, Choat B, Jansen S, López R, Tomášková I, Padilla-Díaz CM, Badel E, Burlett R, King A, *et al.* 2017. Xylem resistance to embolism: presenting a simple diagnostic test for the open vessel artefact. *New Phytologist* **215**: 489–499.

Torres-Ruiz JM, Cochard H, Mayr S, Beikircher B, Diaz-Espejo A, Rodriguez-Dominguez CM, Badel E, Fernández JE. **2014**. Vulnerability to cavitation in *Olea europaea* current-year shoots: further evidence of an open-vessel artifact associated with centrifuge and air-injection techniques. *Physiologia Plantarum* **152**: 465–474.

Torres-Ruiz JM, Cochard H, Mencuccini M, Delzon S, Badel E. **2016**. Direct observation and modelling of embolism spread between xylem conduits: a case study in Scots pine. *Plant, Cell & Environment* **39**: 2774–2785.

Torres-Ruiz JM, Diaz-Espejo A, Perez-Martin A, Hernandez-Santana V. **2015**. Role of hydraulic and chemical signals in leaves, stems and roots in the stomatal behaviour of olive trees under water stress and recovery conditions. *Tree Physiology* **35**: 415–424.

Tyree MT, Ewers FW. **1991**. The hydraulic architecture of trees and other woody plants. *New Phytologist* **119**: 345–360.

Van de Wal BAE, Windt CW, Leroux O, Steppe K. **2017**. Heat girdling does not affect xylem integrity: an *in vivo* magnetic resonance imaging study in the tomato peduncle. *New Phytologist* **215**: 558–568.

Venturas MD, Sperry JS, Hacke UG. **2017**. Plant xylem hydraulics: what we understand, current research, and future challenges. *Journal of Integrative Plant Biology* **59**: 356–389.

Wolf A, Anderegg WRL, Pacala SW. **2016**. Optimal stomatal behavior with competition for water and risk of hydraulic impairment. *Proceedings of the National Academy of Sciences, USA* **113**: E7222–E7230.

Zhang F-P, Brodribb TJ. **2017**. Are flowers vulnerable to xylem cavitation during drought? *Proceedings of the Royal Society B: Biological Sciences* **284**: 20162642.

Zimmermann MH. **1978**. Hydraulic architecture of some diffuse-porous trees. *Canadian Journal of Botany* **56**: 2286–2295.

Zimmermann MH. **1983**. *Xylem structure and the ascent of sap*. Berlin, Heidelberg, Germany: Springer Berlin Heidelberg.

Supporting Information

Additional Supporting Information may be found online in the Supporting Information tab for this article:

Fig. S1 Stem water potential measured with a stem psychrometer vs leaf water potential measured with a Scholander pressure chamber of olive plants monitored for cavitation.
Fig. S2 Spatiotemporal colour maps showing the location and timing of cavitation events monitored in a representative leaf midrib, stem and root of an intact olive seedling using the optical vulnerability method.
Fig. S3 Box plot showing single vessel diameters measured from cross-sections through the root, stem and leaf midrib xylem, and single cavitation event diameters observed using the optical vulnerability method.
Fig. S4 Relationship between leaf midrib P_{50} estimated from six leaves monitored simultaneously for cavitation in an entire olive seedling using a flatbed scanner and their respective distances to the roots.
Fig. S5 P_{50} values estimated from all the roots, stems and leaf midribs monitored for the duration of the experiment.

Please note: Wiley Blackwell are not responsible for the content or functionality of any supporting information supplied by the authors. Any queries (other than missing material) should be directed to the *New Phytologist* Central Office.

Fig. 1 Diagram of an olive seedling showing each of the plant organs monitored for cavitation. (a) Leaf midrib xylem monitored using a camera connected to a light microscope at ×5 magnification. (b) Stem xylem monitored using a custom built OpenSourceOV camera at ×20 magnification. (c) Stem psychrometer installed to record the evolution of stem water potential (Ψ, MPa) over time. (d) Root xylem monitored using a camera connected to a light microscope at ×4 magnification. Right panels represent coloured *Z*-projections of the sum of cumulative embolisms in the (a1) leaf midrib, (b1) stem and (d1) root. These spatiotemporal colour maps depict the location and the timing (transduced as the Ψ recorded by the psychrometer at that time) of xylem cavitation events. Ranges in Ψ that induced cavitation

are shown as a colour scale for each plant organ. The entire montages of colour maps showing the location of cavitation events through time is presented in Supporting Information Fig. S2. Bars: (a, d) 500 µm; (b) 3 mm.

Fig. 2 Optical hydraulic vulnerability curves of leaf midribs (green lines, *n* = 6), stems (blue lines, *n* = 7) and roots (brown lines, *n* = 6), from nine entire olive seedlings. Stem water potential was monitored using a stem psychrometer. The average P_{50} of each plant organ is shown as a dashed black line and ± SE as solid grey lines. Estimates of P_{50} were generated by fitting the Pammenter equation to each curve.

Fig. 3 Differences among the average P_{50} of roots (-7.10 ± 0.62 MPa), stems (-5.67 ± 0.68 MPa) and leaf midribs (-4.76 ± 0.67 MPa) derived by fitting a Pammenter equation to an optical vulnerability curve for each organ from nine monitored olive seedlings. Values are equivalent to black dashed lines in Fig. 2. SE are presented with bars and different letters signify statistically significant differences (one-way ANOVA, post-hoc Tukey, $P < 0.05$).

Fig. 4 Optical hydraulic vulnerability curves of organs monitored simultaneously on the same olive individual (each graph represents one individual). Stem water potential was monitored using a stem psychrometer. Legends in the left of each panel identify the organs monitored for each individual. Additional leaf midribs and stems measured separately in two different individuals are not shown here. Arrows indicate overlapping cavitation events showing cavitation spread between tissues.

Fig. 5 Relationships between the P_{50} of organ pairs from nine monitored olive seedlings. Each data point represents the P_{50} estimated for the two plant organs when simultaneously monitored (*x*- and *y*-axis). Estimates of P_{50} were generated by fitting the Pammenter equation to the optical vulnerability curves presented in Fig. 4.

Fig. 6 Optical hydraulic vulnerability curves of six leaf midribs monitored for embolism accumulation at the same time within a single individual olive seedling using a flatbed scanner. Different symbols represent different leaves and different colours (dark green, dark yellow, light green) represent different branches at different distances from the roots

(closer to further away, respectively). Stem water potential was monitored using a stem psychrometer. The inset box plot shows the variability in leaf midrib P_{50} estimated by fitting the Pammenter equation to the optical vulnerability curves obtained from all the seedlings of the experiment. The range in P_{50} from the six leaf midribs monitored in the same plant ('ind avg', average P_{50} = -6.53 ± 0.34 MPa, green box) was lower but within the range in P_{50} from the leaf midribs of six different seedlings ('spp avg', average P_{50} = -4.76 ± 1.64 MPa, white box). Red lines in the boxes indicate the average P_{50} and black lines indicate the median P_{50}. Each data point shows the P_{50} estimated for each leaf midrib (green points for the leaves of the single seedling and white points for the leaves of different seedlings).

Fig. 7 Relationships between organ-specific P_{50} estimated from optical vulnerability curves of the three olive plant organs (presented in Fig. 2) and xylem dimensions: a metric of xylem vessel resistance to collapse, (a) $(t/b)^3$, (b) the wall thickness of the xylem vessels (t), and (c) the vessel breadth ('b'). Each data point is the average, and ± SE, of 23 to 118 conduits measured from root xylem cross-sections, 85 to 139 conduits from stem xylem cross-sections, and 97 to 150 conduits from leaf midrib cross-sections.

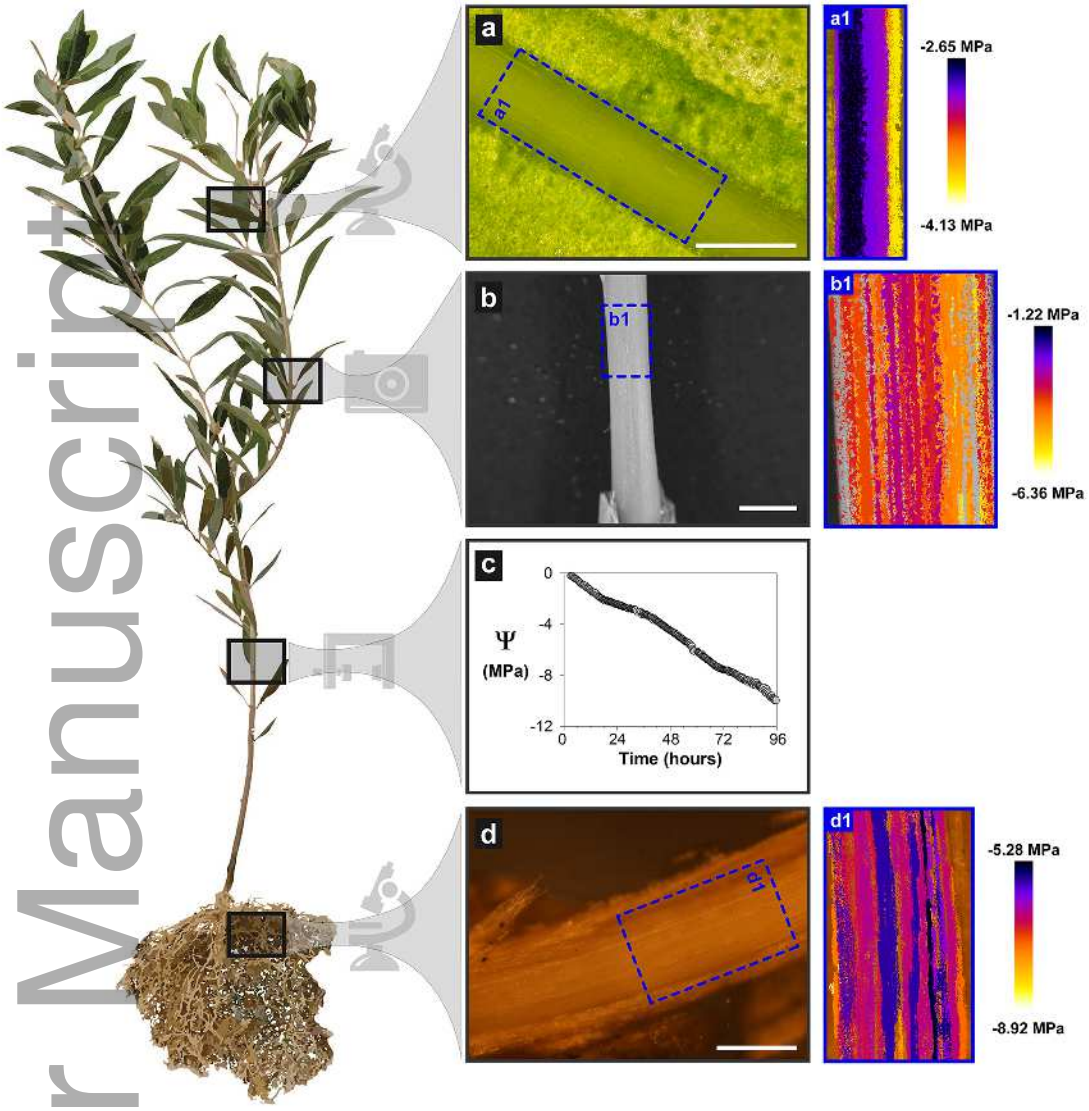

nph_15079_f1.tif

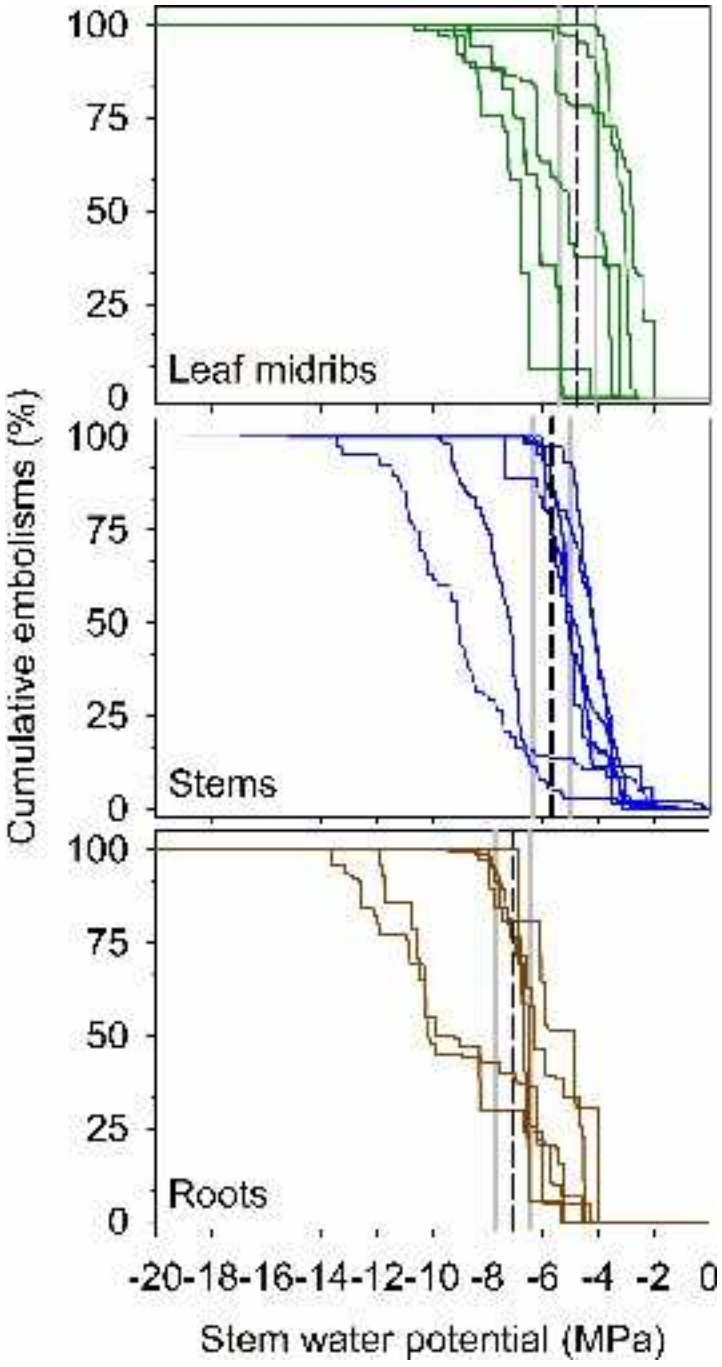

nph_15079_f2.tif

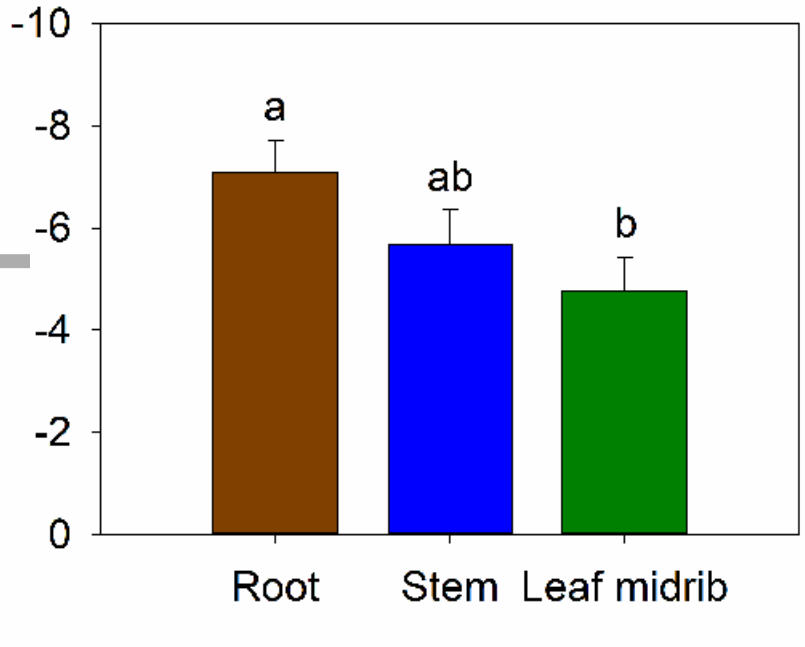

nph_15079_f3.tif

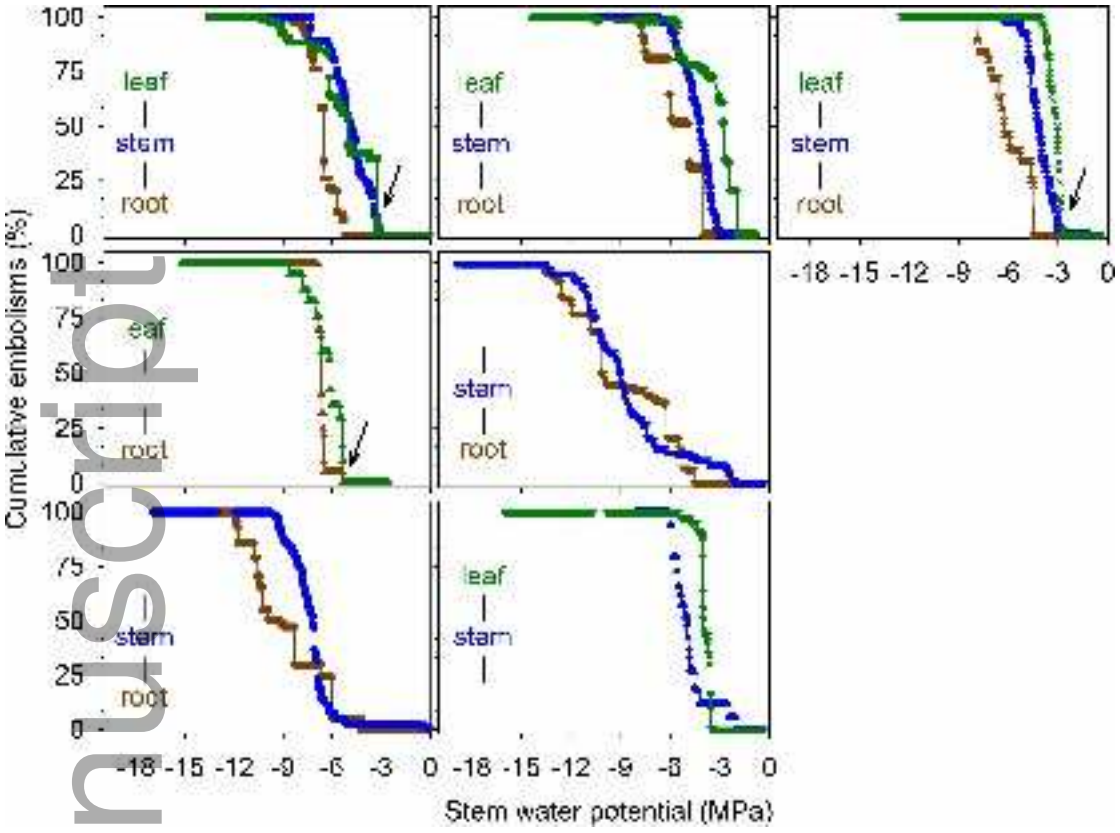

nph_15079_f4.tif

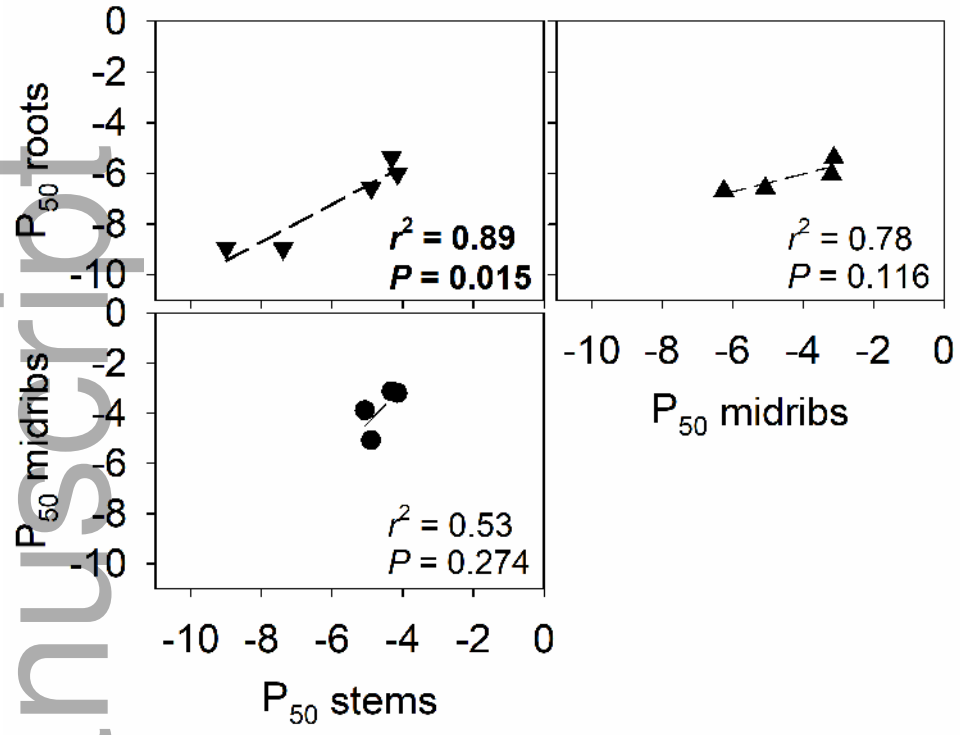

nph_15079_f5.tif

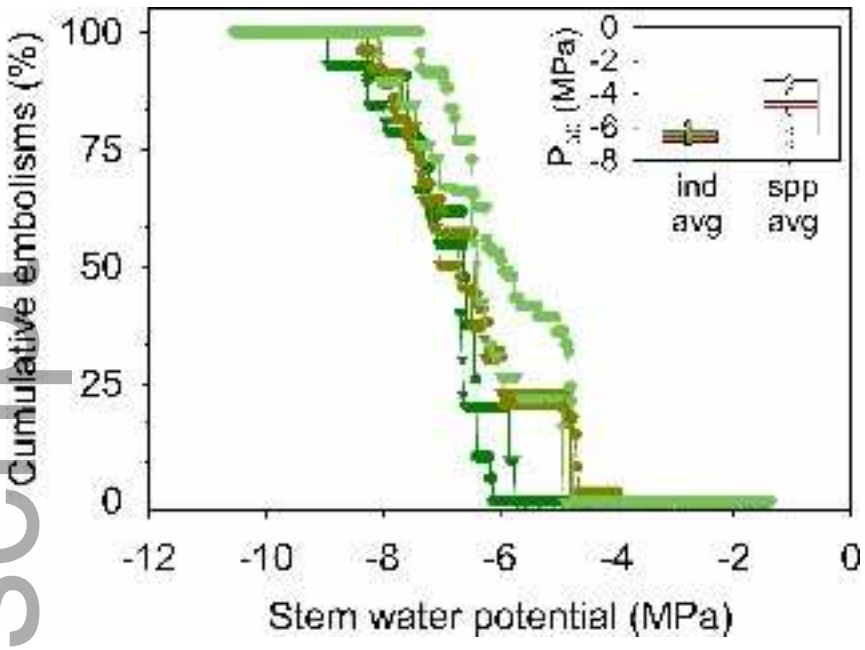

nph_15079_f6.tif

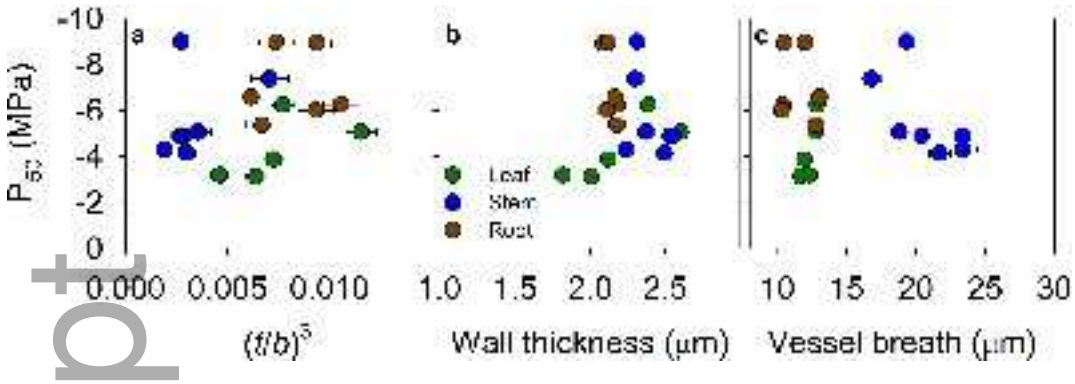

nph_15079_f7.tif